# Lab-on-Fiber Technology: Toward Multifunctional Optical Nanoprobes

**Marco Consales,[†] Armando Ricciardi,[†] Alessio Crescitelli,[†] Emanuela Esposito,[‡,*] Antonello Cutolo,[†] and Andrea Cusano[†,‡,*]**

[†]Optoelectronic Division, Department of Engineering, University of Sannio, I-82100, Benevento, Italy and [‡]CNR-ICIB "E. Caianiello", I-80078 Pozzuoli (NA), Italy. M. Consales and A. Ricciardi contributed equally to this work.

**ABSTRACT**

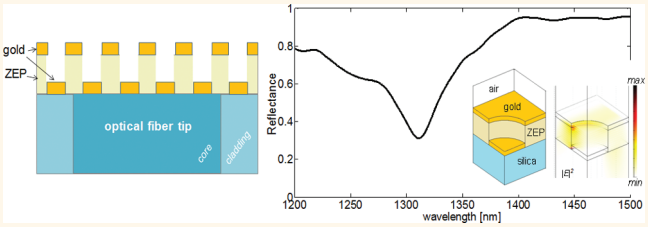


**We propose a reliable fabrication process enabling the integration of dielectric and metallic nanostructures on the tip of optical fibers, thus representing a further step in the "lab-on-fiber" technology roadmap. The proposed fabrication procedure involves conventional deposition and nanopatterning techniques, typically used for planar devices, but here adapted to directly operate on optical fiber tip. Following this approach, we demonstrate a first technological platform based on the integration onto the optical fiber tip of two-dimensional hybrid metallo-dielectric nanostructures supporting localized surface plasmon resonances. By means of experimental measurements and full-wave numerical simulations, we characterize these resonant phenomena and investigate the underlying physics. We show that resonances can be easily tuned by acting on the physical and geometrical parameters of the structure. Moreover, with a view toward possible applications, we present some preliminary results demonstrating how the proposed device can work effectively as an optical probe for label-free chemical and biological sensing as well as a microphone for acoustic wave detection.**

**KEYWORDS:** lab-on-fiber · nanofabrication · fiber optics · localized surface plasmon resonances · metallo-dielectric nanostructures · acoustic wave detection · chemical and biological sensing

The "lab-on-fiber" concept essentially envisages the integration of highly functionalized materials at nano- and microscale within a single optical fiber and aims to develop a novel generation of miniaturized and advanced "all-in-fiber" technological platforms (namely "labs") for both communication and sensing applications.

The lab-on-fiber technology would thus represent the cornerstone of a photonics technological revolution enabling the implementation of fiber-based multifunction sensing and actuating micro- and nanosystems, showing unique advantages in terms of miniaturization, lightweight characteristic, cost effectiveness, robustness, power consumption, and information control. Multifunctional laboratories integrated in a single optical fiber, exchanging information and combining sensorial data, could provide effective autodiagnostic features as well as new photonic and electro-optic functionalities useful in many strategic sectors such as optical processing, environment, life science, safety, and security. The *laboratories* design deals with all those phenomena that provide light manipulation and control at the nanoscale, such as trapping and guiding effects in photonic crystals[1−3] and quasicrystals[4,5] as well as plasmonic nanostructures,[6−9] eventually combined all together in hybrid metallo-dielectric devices.[10−13]

However, the realization of highly integrated optical fiber devices requires that several micro-and nanostructures be fabricated, embedded, and connected all together in order to achieve the necessary light−matter interaction and physical connection. As a consequence, a critical issue to be addressed consists in the definition of a reliable fabrication procedure able to integrate and process, at micro- and nanoscale, several materials with the desired physical, mechanical, magnetic, chemical, and biological properties onto unconventional substrates such as the optical fiber tip.

Promising approaches in this direction were recently introduced;[14,15] the proposed methodology relies on the preventive fabrication of metallic nanostructures on planar silicon wafers by means of electron-beam lithography (EBL), and their successive transfer to small and/or nonconventional substrates (*i.e.*, the fiber tip).[14]

A further method in this direction was also recently demonstrated by the same group through the use of soft lithography and mechanical sectioning, using an ultramicrotome

* Address correspondence to e.esposito@cib.na.cnr.it; a.cusano@unisannio.it.

Received for review December 19, 2011 and accepted March 8, 2012.

**Published online March 08, 2012**
**10.1021/nn204953e**

equipped with a diamond knife; arrays of gold nanostructures embedded in thin epoxy slabs are finally transferred manually to the tip of optical fiber,[15] opening the way to the development of competitive all-fiber localized surface plasmon resonances (LSPRs) and surface-enhanced Raman spectroscopy-based sensing devices. Additional functionalities could also be achieved through the integration of flexible metamaterials.[16]

Following the transferring approach, a monolithic silicon photonic crystal (PC) fiber-tip sensor (for both refractive index and temperature sensing) was recently proposed; it employs a complex combination of EBL and reactive ion etching (RIE) for the structure fabrication and focused ion beam (FIB) milling for the transferring step.[17] A simpler and low cost method based on a UV nanoimprint and transfer lithography (NITL) technique was also introduced.[18] This procedure was applied for the fabrication of optical probes for photonic integrated circuits based on a waveguide-to-fiber gold grating coupler.[18]

Although these methods rely on well-assessed fabrication processes on planar substrates, the final transferring step plays a fundamental role in determining both the fabrication yield and the performance of the final device. This aspect is crucial since it poses severe limitations in the ability to control the transferring procedure at the nanoscale as well as in the adhesive strength of the nanostructures.

To overcome these limitations, alternative approaches based on direct-write patterning of the fiber tip have been explored. The key aspect of these methodologies is to adapt all the standard fabrication processes and tools in terms of material deposition (spin coating, dip coating, sputtering, evaporation, *etc.*), subwavelength patterning, and postprocessing (FIB, EBL, RIE, *etc.*) to operate on the optical fiber tip. However this approach is not straightforward since spin coating and etching procedures are very challenging when they are used on such a substrate.[14,15]

Thus far, only a few direct-writing attempts have been performed,[19,20] in particular for creating metallic nanostructures, giving rise to LSPR effects exploited for chemical and biological sensing. In particular, FIB milling of gold-coated fiber tips has been used to fabricate ordered arrays of apertures with subwavelength dimensions and submicrometer periodicity.[19] Moreover, by using EBL and RIE, ordered arrays of gold nanodots have been fabricated on the fiber tip for biosensing demonstration.[20]

In this work we report on a reliable fabrication process which enables the realization of both dielectric and metallic nanostructures directly on the fiber tip, involving conventional nanotechnology techniques actually specialized to correctly operate on the tip of optical fibers.

## RESULTS AND DISCUSSION

Our fabrication process essentially consists of three main technological steps, as schematically represented in Figure 1a: (i) spin coating deposition of electron-beam resist with accurate thickness control and flat surface over the fiber core region; (ii) EBL nanopatterning; and (iii) superstrate deposition of different functional materials (metallic or nonmetallic) by using various techniques (*e.g.*, sputtering, thermal evaporation, *etc.*), also adapted to operate on an optical fiber tip.

**Customized Spin-Coating Deposition.** It is well-known that the spin-coating process typically produces edge beads around the perimeter of the substrates. This effect is particularly relevant when very small substrates are considered (as in the case of the optical fiber tip), where the edge bead can be as large as the substrate itself thus preventing the use of standard lithographic techniques.[14,15] One of the peculiarities and main innovations of our approach relies on the capability to deposit dielectric layers (and in particular electron beam resist like ZEP 520-A) on the cleaved end of standard optical fibers with controllable thickness and flat surface area in correspondence to the fiber core. To this aim, we adopt a customized spin-coating process involving a rotating chuck *ad hoc* modified in order to host the optical fiber (see Figure 1b). The resist spinning process allows the repeated deposition of ZEP overlays with different thicknesses ranging from 100 to 400 nm depending on the rotating speed (in the range 2000−6000 rpm). The spun resist has uniform areas over the fiber core of about 50−60 $\mu$m in diameter (as shown in Figure 1c). To estimate the ZEP layer thickness and uniformity, we first drilled a hole in the ZEP overlay by using an excimer laser (operating at the wavelength of 248 nm), and then measured the hole depth with an optical profilometer. In Figure 1d and Figure 1e we report two examples of topographic measurements of drilled ZEP overlays characterized by a thickness of approximately 200 and 400 nm, clearly confirming the thickness uniformity over an area of nearly 50−60 $\mu$m in diameter. It is worth noting that the thickness variations in the close proximity of the drilled hole are not due to surface irregularities but only to the ZEP redeposition during the laser ablation process. We point out that the described process can be easily parallelized by making the rotating plate to host more optical fibers, hence enabling a multiple polymer deposition in a single step.

**Dielectric Overlay Patterning and Functional Superstrate Deposition.** Once the dielectric overlay has been deposited, the consequent step relies on its subwavelength patterning by EBL. The optical fiber is lodged on a customized metallic holder allowing a correct exposure process. Moreover, to dissipate the charging effect due to the electron interactions (inevitable when operating on a small glassy substrate), we deposit a metal layer with thickness of about 10 nm on the top of our device. In addition, a special setting of advanced parameters available on the RAITH 150 system is adopted in the exposure procedure to reduce the total

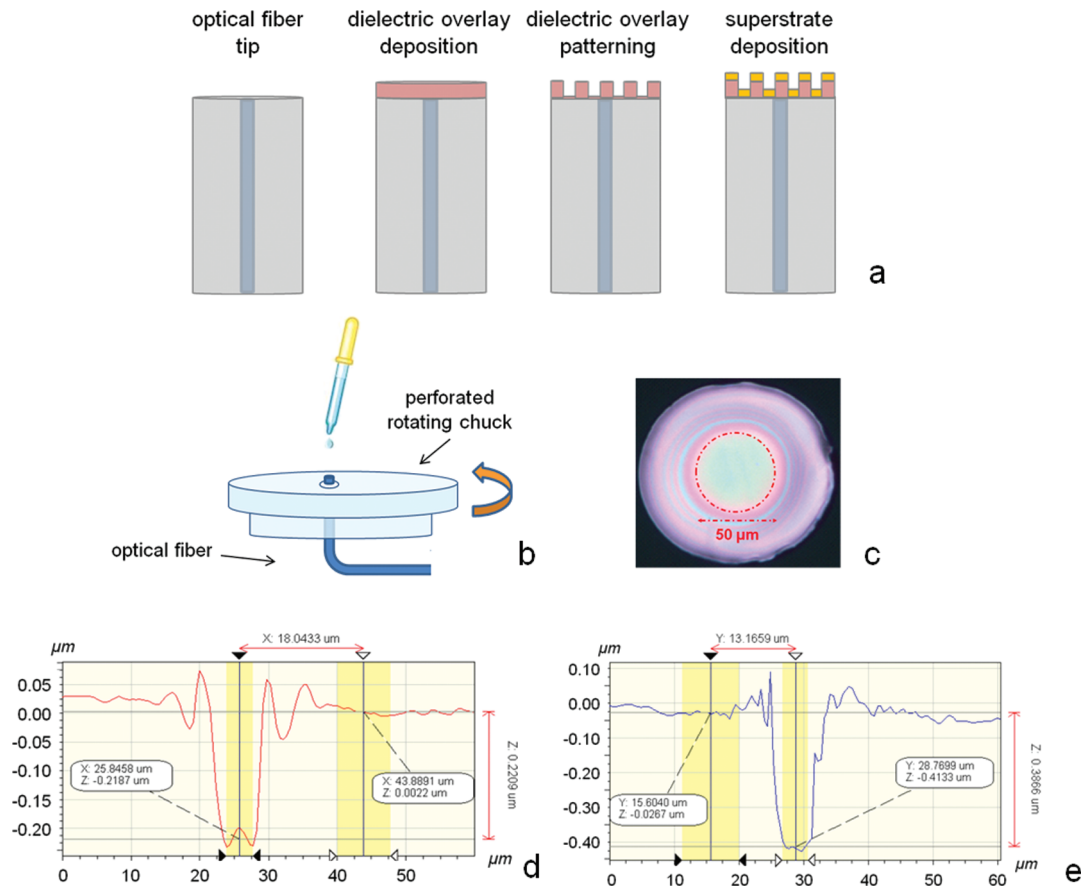


**Figure 1. (a) Schematic (not in scale) of the main technological steps involved in the fabrication path; (b) schematic of the modified spin coater chuck; (c) optical microscope top view image of the fiber tip, coated by a 200 nm-thick ZEP layer; (d, e) cross view topographic characterization results (as retrieved by the optical profilometer) of two perforated ZEP overlays, approximately (d) 200 and (e) 400 nm-thick.**

exposure time. The integration of additional functional (either dielectric or metallic) overlays over the patterned areas could also be carried out by using standard coating techniques (such as sputtering, thermal evaporation, *etc*). Overall, the proposed fabrication–process allows rapid prototyping with a 90% yield, thanks to the reliable spin coating process which makes the substantial difference with respect to the other fabrication processes reported so far; moreover, our nanostructures show good adhesive strength also resulting in reusable devices.

**Structure Design and Analysis.** To test the capability of the proposed fabrication process, we focused the attention on a first technological platform based on a hybrid metallo-dielectric nanostructure supporting LSPRs. The two-dimensional (2D) structure considered in this study is schematically represented in Figure 2a. It essentially consists of a dielectric (ZEP) 200 nm thick layer patterned with a square lattice of holes and covered with a 40 nm thick gold film deposited on both the ridges and the grooves. The lattice period was $a$ = 900 nm, and the holes radius was $r$ = 225 nm, corresponding to a filling factor (radius to period ratio) $r/a$ = 0.25.

When such a structure is illuminated in out-of-plane configuration, as in the case of single mode fiber illumination in the paraxial propagation regime, plasmonic and photonic resonances are expected to be excited due to the phase matching condition between the scattered waves and the modes supported by the hybrid structure, depending on the geometric features of the structure itself.[21] For the numerical analysis we used the commercial software COMSOL Multiphysics (RF module) based on the finite element method.[22] Following the same approach of ref 5, by exploiting the crystal translational and mirror symmetries, the computational domain can be reduced to one-quarter of unit cell, terminated with perfectly electric-conducting (PEC) and vertical perfectly magnetic-conducting (PMC) boundary conditions, placed two-by-two in the opposite walls. The resulting structure (shown in Figure 2b) supports a transverse-electromagnetic (TEM) wave emulating the normally incident plane-wave; we used this kind of excitation instead of a proper fiber mode with Gaussian profile to simplify our simulations. The refractive index data used for modeling both gold and silica in the IR region were taken from ref 23. The ZEP refractive index was taken directly from its data sheet.

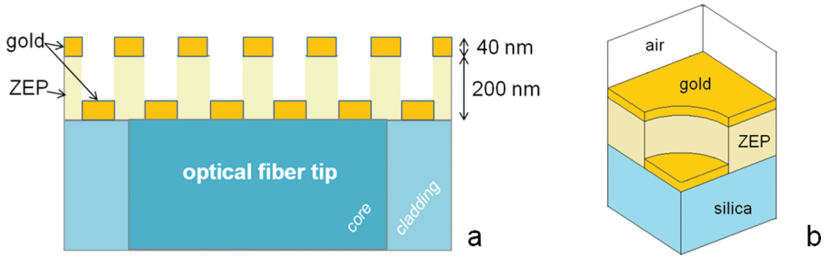


**Figure 2. (a) Schematic (cross section view) of the hybrid metallo-dielectric structure integrated on the optical fiber tip (not in scale); (b) 3D view of $^1/_4$ of unit cell (computational domain).**

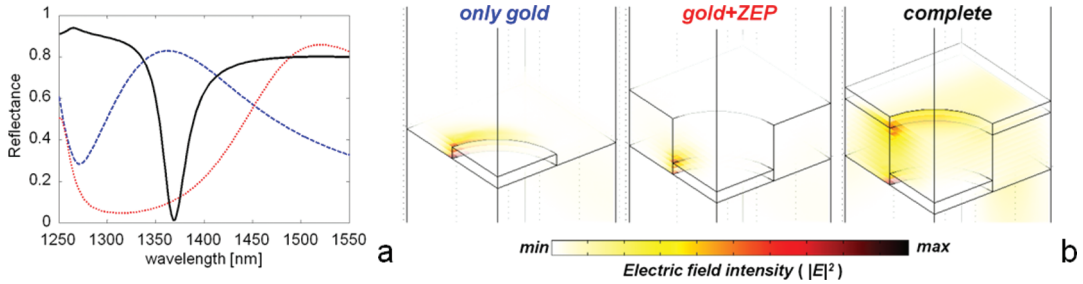


**Figure 3. (a) Theoretical reflectance spectra of the "complete" (solid black), "only gold" (dashed blue) and "gold+ZEP" (dotted red) structures; (b) electric field intensity distributions of the resonant modes evaluated at the reflectance dip/peak wavelengths of the three spectra of (a).**

In Figure 3a we plot the theoretical reflectance spectrum (solid black line) of the hybrid metallo-dielectric fiber-tip device; the high reflectivity baseline is interrupted by a resonance dip centered at 1369 nm with a Q-factor of ~47. To assess the origin of the resonant phenomenon we decided to split up the whole structure into its single parts and separately analyze their contribution to the reflectance spectrum. To this aim, we first calculated the reflectance spectrum of the structure where only the gold nanopillars are present on the fiber tip, which is what we called the "only gold" structure. The result is shown in Figure 3a as a dashed blue curve; a very broad reflectance peak ($Q \approx 8$) appears due to the excitation of LSPR, as in the case of ref 20. Then we calculated the reflectance of the "gold+ZEP" structure, where just the ZEP slab is grown around the gold nanopillars; in this case, the presence of the dielectric medium causes only a reflectance peak red shift of about 158 nm (see the dotted red curve in Figure 3a) according to the modification of the phase matching conditions. Finally, when we consider the "complete" structure (black curve), a significant increase is observed in the reflectance baseline with the creation of a well-defined spectral feature with a *Q* factor significantly higher than those obtained using simply gold pillars.

In Figure 3b the electric field intensity distributions of the resonant modes (evaluated at the reflectance dip/peak wavelengths of the three spectra of Figure 3a) are shown. The maximum electric field intensity value obtained for the "gold+ZEP" structure is ~80% of that relative to the "only gold" one. In contrast to these two cases, for the "complete" structure, the field distribution is significantly different exhibiting two maxima localized around the gold pillars—on the bottom—and the gold slab holes—on the top—(of about 70% and 50% of that relative to the "only gold", respectively), even if it extends across the dielectric layer. Because of the different field distributions, a better comparison can be carried out by considering the electric field intensity enhancement calculated by integrating over the whole structure volume. In doing so, a field enhancement of ~7 was found with respect to the "only gold" and "gold+ZEP" cases. Hence from our analysis it results that the resonant dip in the reflectance spectrum is not merely due to a simple interaction among the single elements constituting the entire structure, thus meaning that the whole is better than the sum of the parts. It is important to underline that in this specific configuration only localized plasmonic modes have been excited in the analyzed spectral range because of the low refractive index value of ZEP. A richer spectrum in terms of resonant dips is expected to be achieved by using higher refractive index material such as silicon or a thicker dielectric layer able to give rise also to the excitation of photonic quasiguided modes (guided resonances).

**Structure Fabrication and Characterization.** The 2D hybrid metallo-dielectric structure was realized by using the previously described fabrication process (fabrication details also available in the "Methods" section).

In Figure 4a and Figure 4b, we show a scanning electron microscope (SEM) image (top view) of the fabricated fiber-tip device and a magnified image of

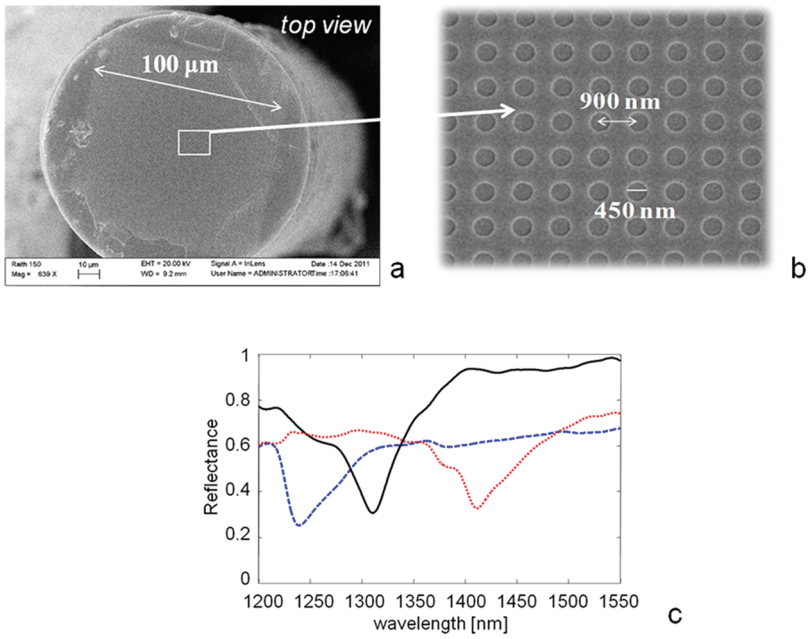


**Figure 4. (a) SEM image of the 100 × 100 $\mu m^2$ matrix of circular holes patterned by the EBL on the ZEP layer; (b) zoomed detail of panel a; (c) measured reflectivity of hybrid metallo-dilectric structures characterized by a period $a$ = 850 (dashed blue curve), $a$ = 900 nm (solid black curve), and $a$ = 1000 nm (dotted red curve).**

the structure, respectively. The lattice periodicity and the hole diameter were estimated to be 900 and 450 nm, respectively.

The measurement setup (details in the Methods section) essentially consists of a 3 dB directional coupler placed between a broadband light source and the optical fiber nanoprobe, with one return end sent to the optical spectrum analyzer. In Figure 4c we show the experimental reflectance spectrum (solid black line) of our device; a resonance dip centered at 1311 nm can be clearly seen, characterized by a *Q*-factor of about 23. From a comparison with the numerical results we note a blue shift of 58 nm, together with a reduction of both the visibility and the *Q*-factor. These discrepancies can be attributed to the fabrication tolerances and to the approximation considered in the numerical analysis where we assumed a plane wave excitation on an *infinite* structure in the periodicity plane.[24] Small polarization effects have also been observed in terms of resonance wavelength shifts and *Q*-factor variation, which can be attributed to the not perfect circularity of the holes. We point out that although no specific parameter optimization was performed, the *Q*-factor exhibited by our hybrid metallo-dielectric structures is larger than most of those observed in typical plasmonic crystal configurations (see Supporting Information of ref 12).

**Resonance Tuning.** Resonant wavelengths can be tailored for the specific application by a suitable choice of the device geometrical parameters such as lattice period, filling factor, dielectric and metal thickness. To demonstrate such a tunability, we designed and fabricated two other samples with different periods (850 and 1000 nm) and the same filling factor ($r$ = 213 nm and $r$ = 250 nm). Since the resonant wavelengths are directly related to the lattice period, a red (blue) shift is expected in case of higher (smaller) lattice pitch. The reflectance spectra of the structures with different periods are reported in Figure 4c (details in the figure caption). As predicted by numerical simulations, we experimentally observed a red shift of about 100 nm and a blue shift of about 70 nm for $a$ = 1000 and $a$ = 850 nm, respectively.

All the results so far reported open up very intriguing scenarios for the development of a novel generation of miniaturized and cost-effective fiber optic nanoprobes useful in many applications including physical, chemical, and biological sensing as well as telecommunications. To show the lab-on-fiber potentiality, in the following we present some preliminary results demonstrating how our nanoprobe is able to sense the refractive index variations in the surrounding environment (suitable for label-free chemical and biological sensing) as well as to detect acoustic waves.

**Refractive Index Measurements.** As previously discussed, the metallo-dielectric nanostructure fabricated onto the fiber tip supports LSPRs, whose excitation wavelengths are very sensitive to variations of the surrounding refractive index.[25] Therefore, a change in the local or bulk refractive index around the fiber-tip device gives rise to a wavelength shift of the resonant peak due to a change of the phase matching condition. Actually, a 40 nm thick gold layer deposited on the top of the fiber-tip device strongly shields the external environment from the plasmonic mode excited within the hybrid crystal, resulting in a very weak sensitivity. To enhance the surface sensitivity of the final device, it is necessary to increase the light-matter interaction with the external environment by properly tailoring the resonant mode field

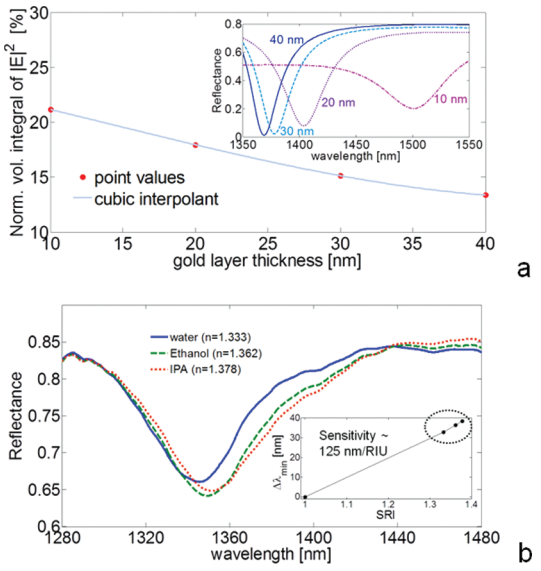


**Figure 5. (a) Volume integral of the electric field intensity ($\iiint |E(r)|^2$ dr) inside the "detection zone" normalized with respect to the integral over the whole structure volume (both accessible and inaccessible for liquids) *versus* the gold layer thickness $t_{Au}$; (inset) theoretical reflectance spectra of the "complete" structure for $t_{Au}$ = 40 nm (dark blue solid line), 30 nm (light blue dashed line), 20 nm (purple dotted line), and 10 nm (magenta dashed-dotted line) are shown. (b) Experimental reflectance spectra for the "complete" structure with $t_{Au}$ = 20 nm immersed in water (solid blue), ethanol (dashed green), and isopropyl alcohol (dotted red); (inset) relative wavelength shifts of the reflection dips as a function of the SRI.**

distribution. To this aim, we can exploit all the degrees of freedom exhibited by the hybrid nanostructures, for example, the lattice design and layer thickness. Here, as proof of principle, we analyze the influence of the gold thickness on the refractive index sensitivity of the fiber device. A numerical analysis has been carried out to estimate the volume integral of the electric field intensity ($\iiint |\mathbf{E}(\mathbf{r})|^2$ d**r**) inside the "detection zone" (*i.e.*, the air holes and the top of the fiber-tip device) as a function of the gold layer thickness. The results, summarized in Figure 5a, clearly show that the maximum electric field intensity (and consequently the enhancing of the light-matter interaction with the surroundings) is achieved when the gold layer thickness is reduced. It is important to emphasize that despite the gold layer thickness reduction, the reflectance dip in the spectrum is still present except for a slight red-shift, a bandwidth widening, and a visibility reduction, as evident from the inset of Figure 5a where the reflectance spectra for $t_{Au}$ = 40 nm (dark blue solid line), 30 nm (light blue dashed line), 20 nm (purple dotted line), and 10 nm (magenta dashed-dotted line) are shown.

Following these results, we fabricated and tested a different sample with a gold layer thickness of only 20 nm (keeping constant the other geometrical parameters, *i.e.*, $a$ = 900 nm, $r$ = 225 nm, and $t_{ZEP}$ = 200 nm). The new sample was then immersed in different liquid solutions such as water ($n$ = 1.333), ethanol ($n$ = 1.362), and isopropyl alcohol ($n$ = 1.378), and the reflectance spectra were measured. The experimental results are shown in Figure 5b, in which the typical red-shift of the curves with increasing values of the surrounding refractive index (SRI) is evident. In particular, in the inset of Figure 5b we plot the relative wavelength shifts of the reflection dips as a function of the SRI. The graph demonstrates a sensitivity of ~125 nm/RIU for detecting changes in the bulk refractive indices of different chemicals surrounding the fiber-tip device.

Another advantage of the proposed nanostructure is represented by its low temperature cross-sensitivity, as demonstrated by experimental measurements (also reported in the "Methods" section) carried out by changing the surrounding temperature from 20 to 60 °C. As a result, a very small resonance shift of approximately 1 nm for a temperature variation of 40 °C was obtained for a device with a 40 nm thick gold superstrate. Finally, the excellent properties of gold for the binding of suitable bioreceptors opens up a plenty of possibilities for novel miniaturized affinity-based biological nanosensors.[26]

We point out that no attempts at this stage have been made to optimize the platform performances. However, by exploiting the degrees of freedom offered when dealing with composite metallo-dielectric nanostructures, some optimization strategies for performance improvement are presently under investigation.

**Acoustic Detection.** As a further application, we also investigated the capability of our LSPR-based fiber-tip device to detect acoustic waves. Indeed, by taking advantage from the typical low Young's modulus of the patterned ZEP, significant variations in the geometrical characteristics of the patterned dielectric slab are expected in response to an applied acoustic pressure wave, hence promoting a consequent shift of the resonant wavelength. It is important to stress, in this case, the fundamental and active role played by the dielectric structure to determine the acoustic performance of the final device.

As proof of principle, preliminary acoustic experiments have been carried out by testing the sample characterized by a period $a$ = 900 nm (whose reflectance spectrum is shown in Figure 4c) using an experimental setup described in detail in the "Methods" section. To gather information about the actual incident acoustic pressure, a reference microphone was placed in close proximity to the fiber sensor. In Figure 6a (upper curve) is reported the typical time response of the fiber nanodevice to a 4kHz acoustic tone with a duration of about 250 ms. For comparison, the response of the reference microphone is also reported in Figure 6a (bottom curve). Data clearly reveal the capability of the in-fiber device to detect acoustic waves in good agreement with the reference microphone. As shown in Figure 6a, the electrical signal is delayed with respect to the optical counterpart, due to the slightly greater distance at which the reference microphone is located from the acoustic source as well

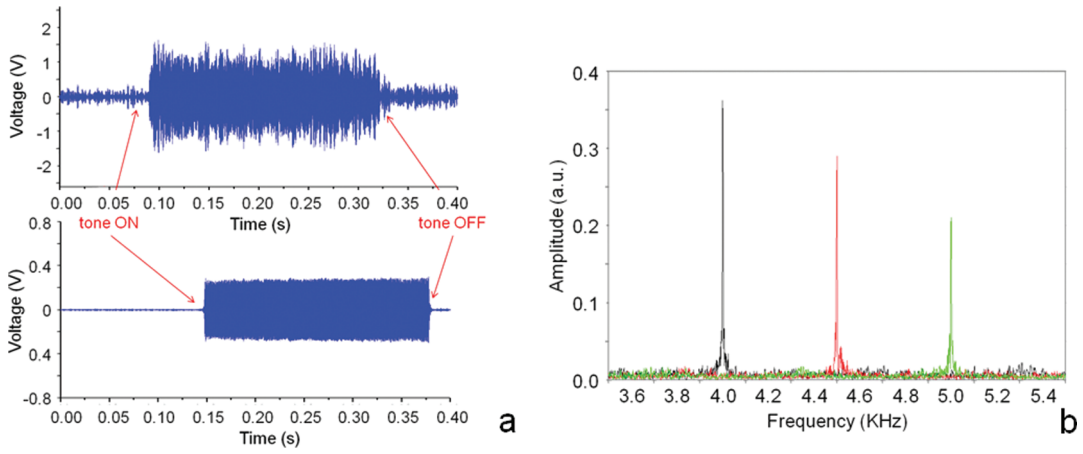


**Figure 6. (a)Typical time responses of the hybrid metallo-dielectric fiber-tip device (top) and reference microphone (bottom) to a 4kHz acoustic pressure pulse with a duration of 250 ms. (b) FFT spectra obtained by the optical fiber sensor in response to three acoustic tones with increasing frequency (4, 4.5, and 5 kHz).**

as to the different electronic processing systems employed. It is also worth noting that, although a relatively high noise level is visible in Figure 6a (the standard deviation of the sensor signal, $\sigma_{noise}$, in the absence of the acoustic wave is nearly 0.1 V), attributable to the instability of the utilized tunable laser, the output voltage of the fiber device was found to be more than an order of magnitude higher than the noise level.

In Figure 6b the FFT spectra obtained by the same optical fiber microphone in response to three acoustic tones with different frequencies (4, 4.5, and 5 kHz) are also shown. The ability of the optical device to discriminate among them is clearly evident. The different amplitude of the sample response to the three tones is due to the different amplification factor applied.

Once again, we emphasize that the above results are only preliminary and no efforts have been made to optimize the performance of the final device. Hence, also in this case, further optimization margins exist through varying the crystal design and metallic layer thickness in order to maximize the dependence of the resonant wavelength on the geometric features of the patterned polymer.

## CONCLUSION

We have demonstrated that by a suitable customization of standard nanoscale deposition and patterning techniques, typically used for planar devices, we were able to define a fabrication process enabling the integration of functional dielectric and metallic nanoscale structures directly on the tip of standard single mode fibers. The effectiveness of the proposed technological process has been confirmed through the realization of a miniaturized fiber-tip device based on a 2D hybrid metallo-dielectric nanostructure supporting LSPR. Both experimental and full-wave numerical analyses have been carried out to characterize the resonant phenomena; the measured *Q*-factors resulted higher than most of those observed in typical plasmonic crystal configurations. We have also shown that the LSPR can be easily tuned by acting on the physical and geometrical parameters of the crystal nanostructure and can be designed to be very sensitive to modifications of the surrounding medium. With a view toward possible applications, we have first presented some preliminary results on the capability of our platform to be used for label-free chemical and biological sensing, showing a bulk sensitivity of about 125 nm/RIU. Finally, we have demonstrated the surprising capability of our device to detect acoustic waves, due to the low elastic modulus of the patterned polymer. Overall, our results demonstrate how the definition of viable lab-on-fiber technologies would enable the realization of technological platforms completely integrated in a single optical fiber, for exploitation in many application fields.

## METHODS

**Device Fabrication.** For the realization of the metallo-dielectric structure schematically represented in Figure 2a, the positive tone electron beam resist ZEP 520A (Zeon Chemicals, refractive index $n \approx 1.54$) was selected as dielectric material, whereas gold was preferred as the metallic superstrate due to its capability of providing high surface plasmon excitation, biocompatibility, and resistance to oxidation degradation. A standard single mode fiber with core and cladding diameters of 9 and 125 $\mu$m, respectively, was used. The fiber tip was first overcoated with a 200 nm-thick layer of ZEP by means of the modified spin-coating technique over which the square lattice (a 100 $\times$ 100 $\mu m^2$ matrix of circular holes with period $a = 900$ nm and radius $r = 225$ nm) has been successively written, by means of an e-beam lithography system (Raith 150). To this aim, the coated fiber end was previously covered by 10 nm gold layer by DC magnetron sputtering in a vacuum system at a pressure of $8 \times 10^{-5}$ Torr, in order to avoid electron charging during the EBL process. We used an acceleration voltage of 20 kV and a

dose of 50 $\mu$C/cm$^2$. After the ZEP developing, a thin film of metallic (*e.g.*, gold, aluminum) and nonmetallic (e.g., $SiO_x$) materials can be deposited in an ultravacuum chamber, with nanometer resolution, by means of DC magnetron sputtering, RF sputtering, and thermal evaporation methods. In our case the realized structure was coated by 40 nm gold layer by DC magnetron sputtering in a vacuum system at a base pressure of $8 \times 10^{-5}$ Torr.

**Setup and Normalization Procedure for Spectral Characterizations.** Spectral reflectance measurements were carried out by illuminating the fiber tip with a broadband optical source (covering the wavelength range 1200−1700 nm) and redirecting the reflected light (*via* a 2 × 1 directional coupler) to an optical spectrum analyzer (Ando AQ6317C). In addition, to compensate for intensity fluctuations, the sample reflectance was normalized by using a fiber-optic reference mirror, fabricated by depositing a 160 nm-thick gold film on the tip of a standard single-mode fiber. The schematic of the characterization setup is reported in the Supporting Information (Figure S1).

**Acoustic Measurements.** For acoustic wave measurements, acoustic excitation was generated by an audio speaker. The sample was interrogated by means of a tunable laser (Thorlabs—INTUN TL1300-B) locked at the spectral edge of the probe resonance, leading to a wavelength intensity conversion when a spectral shift of the resonance occurs. The modulated reflected power is thus delivered through a circulator to a photodetector, and the photogenerated electrical signals are amplified and stored *via* a PC. The schematic of the used setup is reported in the Supporting Information (Figure S3).

*Conflict of Interest:* The authors declare no competing financial interest.

*Acknowledgment.* The kind assistance of D. Iannuzzi (Vrije Universiteit, Amsterdam) and P. Foglia Manzillo (University of Naples "Parthenope") in the profilometric analysis is gratefully acknowledged.

*Supporting Information Available:* Additional information and measurement setups. This material is available free of charge *via* the Internet at http://pubs.acs.org.

*Note Added after ASAP Publication:* After this paper was published online March 16, 2012, a correction was made to Figure 4a. The revised version was reposted April 4, 2012.

## REFERENCES AND NOTES

1. Joannopoulos, J. D.; Johnson, S. G.; Meade, R. D.; Winn, J. N. *Photonic Crystals: Molding the Flow of Light*, 2nd ed.; Princeton University Press: NJ, 2008.
2. Fan, S.; Joannopoulos, J. D. Analysis of Guided Resonances in Photonic Crystal Slabs. *Phys. Rev. B* **2002**, *65*, 235112.
3. Fujita, M.; Takahashi, S.; Tanaka, Y.; Asano, T.; Noda, S. Simultaneous Inhibition and Redistribution of Spontaneous Light Emission in Photonic Crystals. *Science* **2005**, *308*, 1296–1298.
4. Ricciardi, A.; Pisco, M.; Gallina, I.; Campopiano, S.; Galdi, V.; O'Faolain, L.; Krauss, T. F.; Cusano, A. Experimental Evidence of Guided Resonances in Photonic Crystals with Aperiodically-Ordered Supercells. *Opt. Lett.* **2010**, *35*, 3946–3948.
5. Ricciardi, A.; Pisco, M; Cutolo, A.; Cusano, A; O'Faolain, L.; Krauss, T. F.; Castaldi, G.; Galdi, V. Evidence of Guided Resonances in Photonic Quasicrystal Slabs. *Phys. Rev. B* **2011**, *84*, 085135.
6. Halas, N. J. Plasmonics: An Emerging Field Fostered by Nano Letters. *Nano Lett.* **2010**, *10*, 3816–3822.
7. Lassiter, J. B.; Sobhani, H.; Fan, J. A.; Kundu, J.; Capasso, F.; Nordlander, P.; Halas, N. J. Fano Resonances in Plasmonic Nanoclusters: Geometrical and Chemical Tunability. *Nano Lett.* **2010**, *10*, 3184–3189.
8. Schuller, J. A.; Barnard, E. S.; Cai, W.; Jun, Y. C.; White, J. S.; Brongersma, M. L. Plasmonics for Extreme light Concentration and Manipulation. *Nat. Mater.* **2010**, *9*, 193–204.
9. Gopinath, A.; Boriskina, S. V.; Feng, N.-N.; Reinhard, B. M.; Dal Negro, L. Photonic-Plasmonic Scattering Resonances in Deterministic Aperiodic Structures. *Nano Lett.* **2008**, *8*, 2423–2431.
10. Maier, S. A; Atwater, H. A. Plasmonics: Localization and Guiding of Electromagnetic Energy in Metal/Dielectric Structures. *J. Appl. Phys.* **2005**, *98*, 011101.
11. Yao, J.; Le, A.-P.; Gray, S. K.; Moore, J. S.; Rogers, J. A.; Nuzzo, R. G. Functional Nanostructured Plasmonic Materials. *Adv. Mater.* **2010**, *22*, 1102–1110.
12. Yu, X.; Shi, L.; Han, D.; Zi, J.; Paul V. Braun, P. V. High Quality Factor Metallo Dielectric Hybrid Plasmonic−Photonic Crystals. *Adv. Funct. Mater.* **2010**, *20*, 1910–1916.
13. Romanov, S. G.; Korovin, A. V.; Regensburger, A.; Peschel, U. Hybrid Colloidal Plasmonic-Photonic Crystals. *Adv. Mater.* **2011**, *23*, 2515–2533.
14. Smythe, E. J.; Dickey, M. D.; Whitesides, G. M.; Capasso, F. A Technique to Transfer Metallic Nanoscale Patterns to Small and Nonplanar Surfaces. *ACS Nano* **2009**, *3*, 59–65.
15. Lipomi, D. J.; Martinez, R. V.; Kats, M. A.; Kang, S. H.; Kim, P.; Aizenberg, J; Capasso, F.; Whitesides, G. M. Patterning the Tips of Optical Fibers with Metallic Nanostructures Using Nanoskiving. *Nano Lett.* **2011**, *11*, 632–636.
16. Di Falco, A.; Ploschner, M.; Krauss, T. F. Flexible Metamaterials at Visible Wavelengths. *New J. Phys.* **2010**, *12*, 113006.
17. Jung, I. W.; Park, B.; Provine, J.; Howe, R. T.; Solgaard, O. Highly Sensitive Monolithic Silicon Photonic Crystal Fiber Tip Sensor for Simultaneous Measurement of Refractive Index and Temperature. *J. Light. Technol.* **2011**, *29*, 1367–1374.
18. Scheerlinck, S.; Dubruel, P.; Bienstman, P.; Schacht, E.; Van Thourhout, D.; Baets, R. Metal Grating Patterning on Fiber Facets by UV-Based Nano Imprint and Transfer Lithography Using Optical Alignment. *J. Light. Technol.* **2009**, *27*, 1415–1420.
19. Dhawan, A.; Gerhold, M.; Muth, J. Plasmonic Structures Based on Subwavelength Apertures for Chemical and Biological Sensing Applications. *IEEE Sens. J.* **2008**, *8*, 942–950.
20. Lin, Y.; Zou, Y.; Lindquist, R. G. A Reflection-Based Localized Surface Plasmon Resonance Fiber-Optic Probe for Biochemical Sensing. *Biomed Opt Exp.* **2011**, *2*, 478–484.
21. Rosenblatt, D.; Sharon, A.; Friesem, A. A. Resonant Grating Waveguide Structures. *IEEE J. Quantum Electron.* **1997**, *33*, 2038–2059.
22. COMSOL Multiphysics, RF User's Guide, version 3.5a; Comsol AB: Stockholm, Sweden, 2008.
23. Palik, E. D. *Handbook of Optical Constants of Solids*; Academic Press: Orlando, FL, 1985.
24. Peters, D. W.; Kemme, S. A.; Hadley, G. R. Effect of Finite Grating, Waveguide Width, and End-Facet Geometry on Resonant Subwavelength Grating Reflectivity. *JOSA A* **2004**, *21*, 981–987.
25. Stewart, M. E.; Anderton, C. R.; Thompson, L. B.; Maria, J.; Gray, S. K.; Rogers, J. A.; Nuzzo, R. G. Nanostructured Plasmonic Sensors. *Chem. Rev.* **2008**, *108*, 494–521.
26. Anker, J. N.; Hall, W. P.; Lyandres, O.; Shah, N. C.; Zhao, J.; Van Duyne, R. P. Biosensing with Plasmonic Nanosensors. *Nat. Mater.* **2008**, *7*, 442–453.